UNCERTAINTY ANALYSIS ON REACTIVITY AND DISCHARGED INVENTORY DUE TO $^{235,238}U$, $^{239,240,241}Pu$, AND FISSION PRODUCTS: APPLICATION TO A PRESSURIZED WATER REACTOR FUEL ASSEMBLY

FUEL CYCLE AND MANAGEMENT

KEYWORDS: *uncertainty, nuclear data, inventory*

D. F. DA CRUZ,* D. ROCHMAN, and A. J. KONING

Nuclear Research and Consultancy Group NRG, P.O. Box 25, 1755 ZG Petten, The Netherlands

Received November 5, 2012
Accepted for Publication June 18, 2013
http://dx.doi.org/10.13182/NT12-154

Uncertainty analysis on reactivity and discharged inventory for a typical pressurized water reactor fuel element as a result of uncertainties in $^{235,238}U$, $^{239,240,241}Pu$, and fission products nuclear data was performed. A typical Westinghouse three-loop fuel assembly fueled with UO_2 fuel with 4.8% enrichment was selected. The Total Monte Carlo method was applied using the deterministic transport code DRAGON. This code allows the generation of the few-groups nuclear data libraries by directly using data contained in the nuclear data evaluation files. The nuclear data used in this study are from the JEFF3.1 evaluation, with the exception of the nuclear data files for U, Pu, and fission products isotopes (randomized for the generation of the various DRAGON libraries). These are taken from the TALYS evaluated nuclear data library TENDL-2012. Results show that the calculated total uncertainty in k_{eff} (as a result of uncertainties in nuclear data of the considered isotopes) is virtually independent of fuel burnup, and amounts to 700 pcm. The uncertainties in the inventory of the discharged fuel are dependent on the element considered and lie in the range 1% to 15% for most fission products, and are $<5\%$ for the most important actinides. The total uncertainty on the reactor parameters was also split into different components (different nuclear reaction channels), and the main sources of uncertainties were identified.

Note: Some figures in this paper may be in color only in the electronic version.

I. INTRODUCTION

For decades, several deterministic approaches were followed to propagate uncertainties from nuclear data to reactor physics parameters, methods that relied on perturbation theory (see, for instance, Ref. 1). In these methods, both sensitivity profiles and covariance data need to be combined to obtain final uncertainties. Recently, an extensive study[2,3] based on these methods has been performed to assess the sensitivity and uncertainty due to nuclear data uncertainties of key integral reactor parameters, applied to several types of advanced nuclear systems. The Total Monte Carlo (TMC) method[4] in its turn is a Monte Carlo–based technique developed at the Nuclear Research and Consultancy Group (NRG) and relies on the higher computational power available nowadays. TMC involves a large number of calculations for the same model performed with different nuclear data in each of them, and therefore bypasses the various covariance processing codes required in the deterministic approach. So far, these numerous

*E-mail: dacruz@nrg.eu

calculations required by TMC were performed using a Monte Carlo transport code system such as SERPENT (Ref. 5) and MCNP (Ref. 6). This was demonstrated in a previous study,[7] where TMC was applied to a burnup calculation of a pressurized water reactor (PWR) fuel assembly to determine uncertainty in reactivity, discharged inventory, and radiotoxicity as results of global variations in nuclear data of major actinide isotopes.

Sensitivity studies are of great importance in reactor physics, in relation to safety analyses. For sensitivity studies, the global variations in cross sections have to be cut into the several reaction channel components, and even into distinct energy ranges. The main purpose is to identify the main sources of uncertainties, so that special attention can be devoted to the improvement of data corresponding to the particular nuclear reaction channel and isotope. For these studies, the effects in reactor parameters would be small and mostly of the same order of the statistical uncertainties inherent in Monte Carlo calculations. In this case, applying TMC with MCNP or SERPENT would not be feasible. This problem can be remedied by replacing the Monte Carlo transport code by a deterministic transport code. In a recent study,[8] the Monte Carlo transport code was replaced by the deterministic cell code DRAGON, and the uncertainties in nuclear data of ^{235,238}U were propagated for a burnup calculation of a PWR fuel assembly model. The same approach is followed in this work, however, considering a larger number of isotopes that could influence the total uncertainties.

In this paper, the model of the PWR fuel assembly, the TMC methodology, and the code system are first presented. In the second part of the paper, results are presented for the uncertainty in reactivity and discharged inventory, where the importance of the different reaction channels and nuclear parameters are discussed. The paper is then finalized with conclusions and prospects for future work.

II. ASSEMBLY MODEL

A single assembly used in a Westinghouse three-loop reactor[9] was considered in this study. Table I includes some of the main specifications of the assembly model. This 17×17 assembly is filled with UO_2 fuel, with an enrichment of 4.8%. The calculations were performed with a boric acid concentration in the coolant of 500 ppm, corresponding to an average concentration during the lifetime of the assembly in the reactor. The temperature of the fuel is assumed to be 930 K, and that of the cladding and coolant is 586 K. The assembly is depleted up to 60 GWd/tonne HM, according to the procedure discussed in Sec. III. The assembly is supposed to be discharged from the reactor at burnup of 50 GWd/tonne HM. At this burnup level, the analysis of the discharged inventory is carried out.

TABLE I

Main Specifications of the Westinghouse Three-Loop Fuel Assembly Model*

Parameter	Value
Configuration	17×17 square bundle
No. of fuel rods	264
Guide + instr. tubes	25
Pin pitch	1.26 cm
Pellet diameter	0.82 cm
Clad thickness	0.06 cm
Clad outer diameter	0.95 cm
Clad material	Zirconium
Assembly pitch	21.5 cm
Power density	39 W/g HM

*Reference 8.

III. METHODOLOGY AND CODE SYSTEM

For the determination of the uncertainty on the reactivity and discharged inventory of the described assembly, due to uncertainties in nuclear data, we selected the TMC method. This relatively new method was developed at NRG (Ref. 4) as an alternative to the more cumbersome perturbation methods used so far extensively over the world.

The TMC method consists of performing a large number of the same calculations [in our case, the neutron flux calculations and depletion with the cell code DRAGON (Refs. 10 and 11)], where the only difference between these individual calculations is the random change of one single nuclear model parameter (or a set of parameters) within some predefined boundaries, leading to an entire random nuclear data library. By performing statistical analysis of the final results, one can determine the different moments and infer the final uncertainty in the studied parameters, as a first approximation to the solution of the likelihood equations. The complete calculation scheme is shown in Fig. 1.

III.A. Randomized Nuclear Data

The chosen parameters to be randomized are nuclear data parameters for the most important actinide isotopes (^{235}U, ^{238}U, ^{239}Pu, ^{240}Pu, and ^{241}Pu) and fission products. The list of fission products considered comprises the most important isotopes, and has been taken from Ref. 12. Within the WIMS-D library update project from the International Atomic Energy Agency, a list of the most important fission products has been compiled, both of explicitly represented (56 nuclides) and 79 nuclides, which are usually lumped together (and called a lumped fission product). The selection criteria were extensively discussed in Ref. 12, and are based on their lifetime and

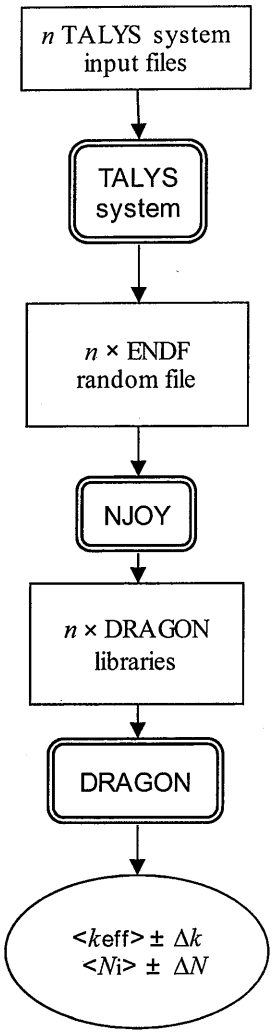

Fig. 1. Flowchart of the calculation scheme for the uncertainty propagation with the TMC method. N = concentration of the different isotopes.

absorption potential. From this list of 135 nuclides, we excluded the natural isotopes of Zr, and the isotopes ^{148m}Pm and ^{127m}Te. The natural Zr isotopes were excluded from the list since the cladding is composed of 100% Zr, and we want to consider Zr isotopes produced only as fission products. A total of 128 isotopes were considered in the current study. In the Appendix, Table A.I gives a list of these isotopes.

The list of randomized nuclear data parameters can include cross sections, $\bar{\nu}$ (average number of produced neutrons per fission), energy per fission, angular and energy distributions, resonance information, etc. These are parameters contained in the nuclear evaluation files. The evaluation files in ENDF-6 (Evaluated Nuclear Data File-6) format used for all nuclides in this study were the JEFF3.1 evaluation files, except for the isotopes being randomized. The evaluation files for these randomized isotopes were produced with the TALYS nuclear reactions code system,[13] according to a procedure described in a few dedicated papers.[4,14] A total of 20 to 30 theoretical parameters are varied within predetermined ranges to create TALYS inputs. With the addition of a large number of random resonance parameters, nuclear reactions from thermal energy up to 20 MeV are covered. The justification for the choices of theoretical parameters and their variations is extensively described in a dedicated publication.[15] The TALYS system creates random ENDF nuclear data files based on these random inputs, according to the procedure also described in Ref. 15. The ENDF random files contain nuclear data stored in different subsections (identified in ENDF language by different Material File, or MF numbers); for example:

1. MF1: contains the number of neutrons produced per fission $\bar{\nu}$ and the energy released per fission
2. MF2: contains resonance parameters for all reaction channels, including fission, capture, and scattering (starting at 10^{-5} eV up to 2.25 keV for ^{235}U and 20 keV for ^{238}U, for example)
3. MF3: cross sections for all reaction channels in the fast neutron energy range
4. MF4: angular distributions
5. MF5: fission neutron spectrum
6. MF6: double differential data.

Approximately 1000 random files were generated for each separate MF number, and another 1000 random files for variations in all MF numbers simultaneously, and for each considered isotope (actinides and fission products). For some MF numbers, random files were also produced where only a single reaction channel or resonance parameter was changed.

Also taken into account in this study were variations in fission products yields for the fissile isotopes considered during the depletion calculations. As explained in a previous publication,[16] the fission yields are obtained from the TAFIS code (one of the codes within the TALYS code system) and normalized to the ENDF/B-VII.0 yields and uncertainties. If a yield (and its uncertainty) is present in ENDF/B-VII.0, it is used in this work, and otherwise, the Wahl systematics are used[17] with a limit of 100% for the uncertainties (the original Wahl systematics give uncertainties up to 10 000%).

III.B. Processing with NJOY

Before these random nuclear data evaluation files can be used to simulate the neutron transport with the code DRAGON, they are processed by the code NJOY (Ref. 18) (version 99.125). This modular code for nuclear data processing basically reads the evaluation file,

processes it at requested temperatures and dilution values, collapses the data to a few-group energy grid, and writes the data into a format used by DRAGON. A 172-energy-group XMAS (Ref. 19) structure was selected for this study. The source of NJOY was appended with an extra module DRAGR, which writes the processed nuclear data into the unique format of the DRAGON library, called DRAGLIB.

The program PyNjoy (also included in the DRAGON package) takes care of the automation of the production of the partial DRAGON libraries (based on the randomized ENDF files) and the appending to the basic DRAGON library. The basic DRAGON library contains all isotopes that are not being randomized and are based on JEFF3.1 evaluation files. In the case of the fission products being considered, the corresponding randomized DRAGON libraries were produced by changing simultaneously the nuclear data for all 128 isotopes.

III.C. DRAGON Calculation Scheme

The simulation of the assembly was modeled with the modular code DRAGON (Refs. 10 and 11) version 4.0. DRAGON is a lattice cell code that allows the simulation of a large diversity of thermal systems as well as fast spectrum systems. It can simulate the neutron transport in a unit cell or a fuel assembly. Several algorithms are available to solve the neutron transport equations, like the method of collision probabilities, the interface-current method, or the long characteristics method. It also includes modules for interpolation of microscopic cross sections, resonance self-shielding calculations, editing of condensed and homogenized quantities, and isotopic depletion calculations. Microscopic libraries in different standard formats can be accessed by DRAGON, apart from the unique indigenous DRAGLIB format.

An octant of the fuel assembly was modeled in DRAGON, assuming symmetry. Reflective boundaries are considered at the outer boundaries, and in the axial direction, the model is infinite. The 39 fuel rods in the model are grouped into 5 fuel rod types, depending on a rod's position relative to the guide tubes and the outer assembly boundary. The self-shielding of the microscopic cross sections is performed using the subgroup method, and the physical probability tables are calculated using the temperature-interpolated cross-section data. Only linearly anisotropic scattering is considered.

The assembly calculations are performed at two levels. At the first level, each pin-cell has a single mesh in the x- and y-directions, and each fuel region is subdivided into five annular regions. The calculations are done in 172 energy groups (XMAS group structure) and using the collision probability technique, where linearly anisotropic components of the intercell current are used. The linear system of multigroup collision probability is solved for the critical buckling, and the multigroup neutron flux is calculated. This is followed by condensation of the cross sections into 26 groups. The second-level calculation is carried out with the data in 26 energy groups, and with a modified geometry with a finer meshing in the x- and y-directions. The method of characteristics is applied, and the system matrix is solved for the effective multiplication factor using the buckling value determined in the first-level calculation.

Depletion is performed under constant fuel power in small burnup steps, and considering the energy released in the complete geometry. After each step, the concentrations are updated in the library and a new self-shielding process is started followed by the flux calculations in the two levels as described above. The nuclear data used in the depletion module are the same as in the transport calculations.

The number of energy groups chosen for the DRAGON libraries (and its multigroup structure) is considered adequate for this study. Although the central values of the integral parameters studied are affected by the choice of multigroup structure, the uncertainties on these values are hardly sensitive to it and represent only a second-order effect. For example, the multigroup structure effect on the uncertainty in the multiplication factor due to variations in ^{235}U nuclear data amounts to 20 to 40 pcm (4% to 10% relative to the uncertainty in the multiplication factor), when going from a 172-group XMAS structure to a 361-group SHEM structure.[20]

IV. RESULTS

Uncertainties in multiplication factor (k_{eff}) and discharged inventory (at 50 GWd/tonne HM) as a result of uncertainties in nuclear data for U and Pu isotopes and fission products are obtained with the procedure described in Sec. III.

IV.A. Uncertainties in Nuclear Data

From the 1000 random ENDF files generated with the TALYS code system, the uncertainties associated with the different reaction channels can be extracted. Figure 2 shows these uncertainties for some important reaction channels of ^{235}U and ^{238}U, and for the uncertainty in $\bar{\nu}$. Figure 3 includes the same data for the Pu isotopes. Data are shown for energies up to the end of the resonance range. These data are going to be included in the TALYS Evaluated Nuclear Data Library TENDL-2012 (Ref. 21) in the form of covariance data in files MF32 (resonance parameter covariances) and MF33 (cross-section covariances).

As explained in Ref. 14, the predefined ranges of variation of the nuclear parameters in the TALYS system were such that they matched experimental uncertainty data from the EXFOR database[22] and the uncertainty values in existing publications (such as, for instance, the

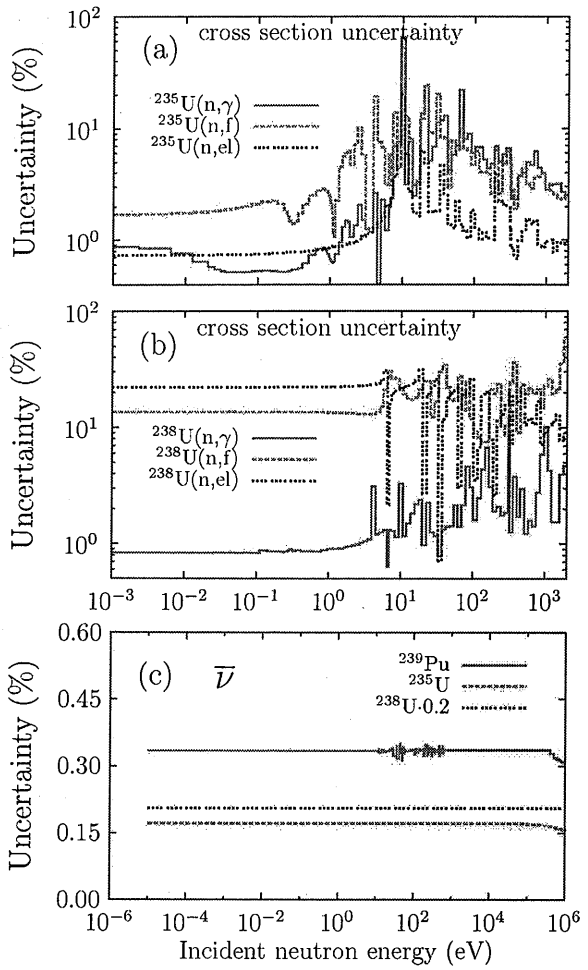

Fig. 2. Uncertainty in cross sections for the main reaction channels for (a) ^{235}U and (b) ^{238}U, and (c) the number of neutrons produced per fission ($\overline{\nu}$) as applied in this study.

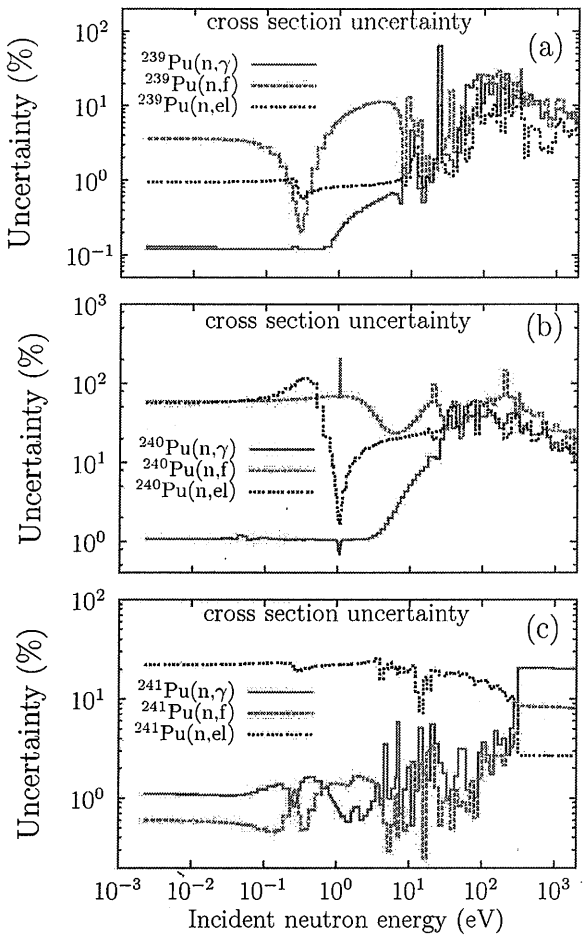

Fig. 3. Uncertainty in cross sections for the main reaction channels for (a) ^{239}Pu, (b) ^{240}Pu, and (c) ^{241}Pu as applied in this study.

Atlas of Neutron Resonances[23]). For nuclear data for which no experimental data (or relevant publication) were available, the systematics as described elsewhere[14,24] were used for the choice of range of corresponding theoretical nuclear parameters.

IV.B. Reactivity Swing

Although 1000 random ENDF files were available, a lower number of files were used in the uncertainty analysis. The convergence of the k_{eff} distribution was tested by analyzing the first three moments: average, standard deviation, and skewness. Figure 4 presents an example of the graphs for the updated averaged uncertainty and skewness, and the distribution of k_{eff} values.

In general, 500 to 550 random files were considered for the results presented here.

Figure 5 includes the results obtained for the uncertainty in the effective multiplication factor as a function of the fuel burnup for variations in both ^{235}U and ^{238}U nuclear data, and their fission yields. In both these graphs, only the nuclear data corresponding to the particular isotope were varied. The curve labeled as transport data was obtained by varying simultaneously all MF numbers in the ENDF files; therefore, all transport data changes. The other curves represent the contributions of the different components separately. Also included in these graphs is a curve for the uncertainty due to variations in fission yields exclusively.

IV.B.1. Uranium Isotopes

The uncertainty due to the variations in ^{235}U transport data decreases monotonically with time. As ^{235}U fissions and decreases in concentration toward the end of life (EOL), the importance of the cross-section values for this actinide also decreases. Toward EOL, fissile actinides like

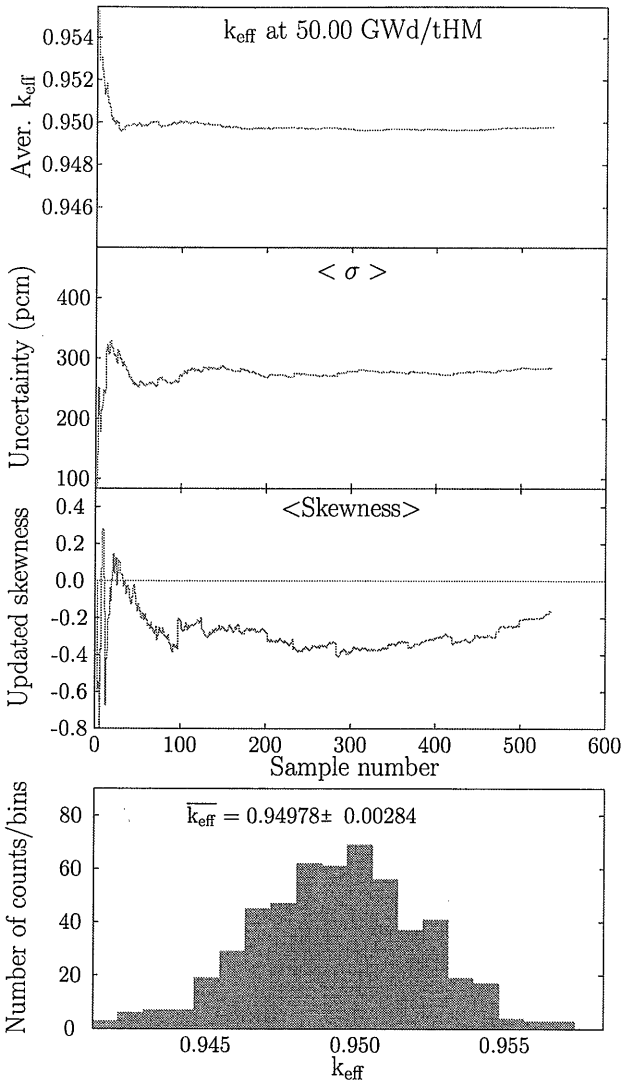

Fig. 4. Example of convergence of k_{eff} distribution at 50 GWd/tonne HM in the case of changing ^{235}U nuclear data. Three moments of the distribution are presented: the average, standard deviation, and skewness.

^{239}Pu start to play an important role. On the other hand, the uncertainty due to variations in fission yields of ^{235}U starts at zero (since there are no fission products present in the fuel at zero burnup) and increases with burnup to a maximum at 40 GWd/tonne HM, and decreases slightly until the EOL. Figure 5 shows that the largest effect on the total uncertainty from transport data is from uncertainties in the fission cross section in the resonance range. At second place, the uncertainty due to the variations in $\bar{\nu}$ plays a role. This parameter is important in the total neutron balance, directly reflected in the effective multiplication factor. As depicted in Fig. 2, the considered uncertainty in ^{235}U thermal $\bar{\nu}$ amounts to $\sim 0.17\%$, a value that is considerably lower than the uncertainty in ^{235}U thermal fission cross section (1.9%).

The uncertainty due to variations in ^{238}U transport data shows a different behavior. At zero burnup, it shows the maximum value and decreases until ~ 45 GWd/tonne HM, and starts to increase again toward the EOL. This behavior can be understood by analyzing the different partial contributions. One would expect that the resonance region data (more specifically, the radiative capture cross section) would be the major contribution over the entire burnup time. That is not the case. It constitutes the major contribution at beginning of life (BOL) and up to ~ 40 GWd/tonne HM, and then it decreases steadily and reaches a minimum at ~ 50 GWd/tonne HM. This trend can be explained as follows. At BOL, ^{238}U is the main source of neutron absorption and ^{235}U is the main source of neutron production. These two contributors to the multiplication factor are quite uncorrelated, in the sense that changes in resonant absorption of ^{238}U do not affect the production of neutrons by ^{235}U. However, for higher fuel burnup values, ^{239}Np (and consequently ^{239}Pu) are being bred by neutron capture of ^{238}U isotopes. ^{239}Pu is a good source of neutrons by fission, and therefore as the amount of ^{239}Pu increases with burnup, the neutron production by fission of ^{239}Pu increases steadily. This effect is partly going to counterbalance the absorption of neutrons by ^{238}U, with a concentration that is virtually constant during the assembly lifetime. In conclusion, changes in the resonance capture of ^{238}U may increase the neutron absorption (and decrease k_{eff}), but at the same time, a larger amount of neutrons is going to be produced by ^{239}Pu, which compensates the neutron absorption effect at a certain concentration of ^{239}Pu (which is constantly being bred).

For this particular fuel composition and uranium enrichment, the two effects cancel each other at ~ 50 GWd/tonne HM. The situation will probably be different for a different fuel composition, and breeding ratio of ^{239}Pu. The second largest contribution, and the most important at higher burnup, comes from variations in $\bar{\nu}$, although fast fission of ^{238}U does not represent a large contribution to the total fission rate. The considered uncertainty in ^{238}U thermal $\bar{\nu}$ amounts to $\sim 1\%$, a comparable value to the uncertainty in ^{238}U thermal fission cross section (0.9%).

IV.B.2. Plutonium Isotopes

For the Pu isotopes, the effect on the uncertainty in k_{eff} is different (Fig. 6) since the Pu isotopes are not present in the fuel at the beginning of the irradiation. We should call attention to the difference in scale of the y-axis between the different graphs in Fig. 6. At zero burnup, the effect due to uncertainties in transport data and fission yields is zero. As the Pu isotopes build up, their importance increases monotonically with burnup. The contribution due to the uncertainties in data from ^{239}Pu is the largest, followed by that from ^{241}Pu and a small contribution from ^{240}Pu.

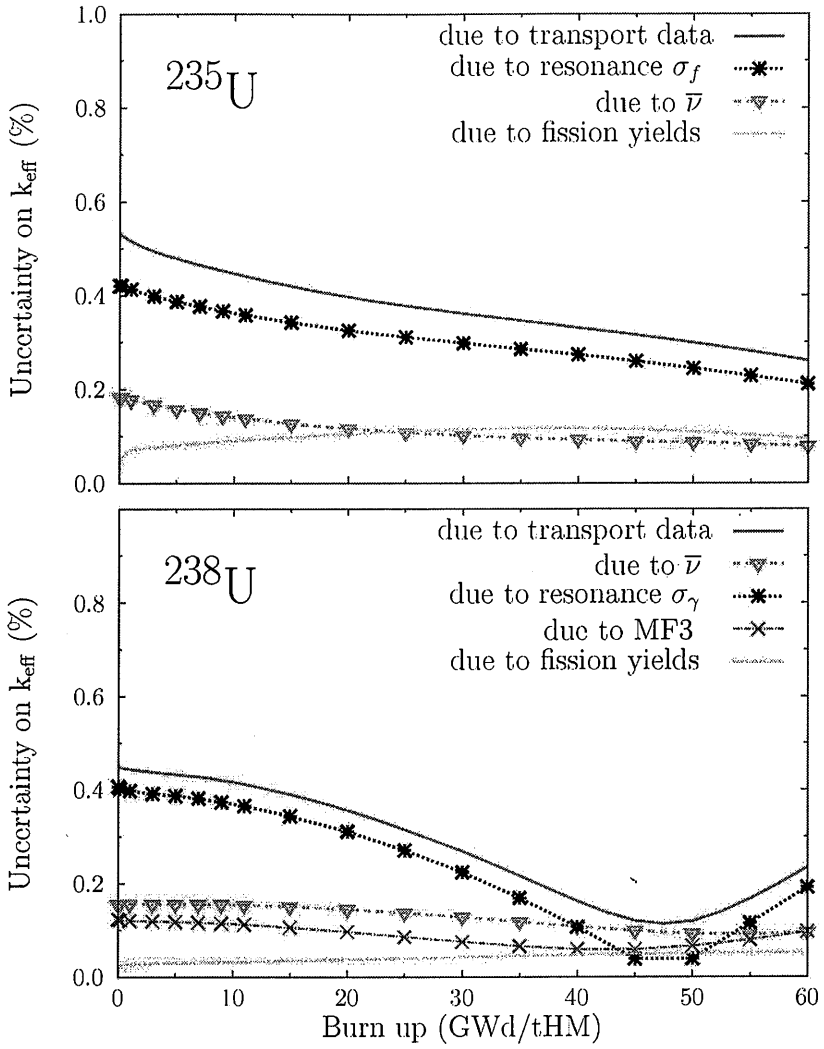

Fig. 5. Uncertainty on k_{eff} as a function of burnup, for variations in the nuclear data of ^{235}U and ^{238}U. The different curves refer to variations in specific parts of the nuclear data. The curve labeled transport data refers to variations in all nuclear data, excluding fission yields.

For ^{239}Pu, the largest contribution to the uncertainty in reactivity is due to variations in transport data, although the contribution of deviations in fission yields is not negligible: 454 pcm due to transport data, and 178 pcm due to fission yields, both values at EOL. When breaking up the uncertainty due to transport data, the largest contribution is by $>85\%$ due to variations in data on MF2, more specifically in fission cross-section data in the resonance and thermal energy range. The second largest contribution is due to variations in $\bar{\nu}$ data. Toward the fuel EOL, the total uncertainty seems to tend to a saturation value, although at a burnup value higher than 60 GWd/tonne HM. The concentration of ^{239}Pu in the fuel reaches a maximum value at ~ 50 GWd/tonne HM. As displayed in Fig. 3, the uncertainty in thermal fission cross section (at the lowest point of the resonance peak at 0.4 eV) amounts to $\sim 0.2\%$ to $\sim 0.3\%$, in contrast to an uncertainty of $\sim 1.0\%$ in the ^{239}Pu thermal $\bar{\nu}$ (Fig. 2).

For ^{240}Pu, the largest contribution is due to variations in the resonance parameter Γ_γ, which also affects other cross sections in the resonance range and not exclusively the resonance capture cross section. This feature is inherent to the application in TALYS of the multilevel Breit-Wigner nuclear model, which better describes the cross sections at the resonance range for ^{240}Pu. However, changes in Γ_γ for ^{240}Pu influence mainly the radiative capture since the fission cross section is quite small at thermal energies. The total contribution at 50 GWd/tonne HM is 43 pcm.

For ^{241}Pu, analog to ^{239}Pu, the largest contributor to the uncertainties in reactivity is from transport data (88 pcm), followed by the fission yields contribution

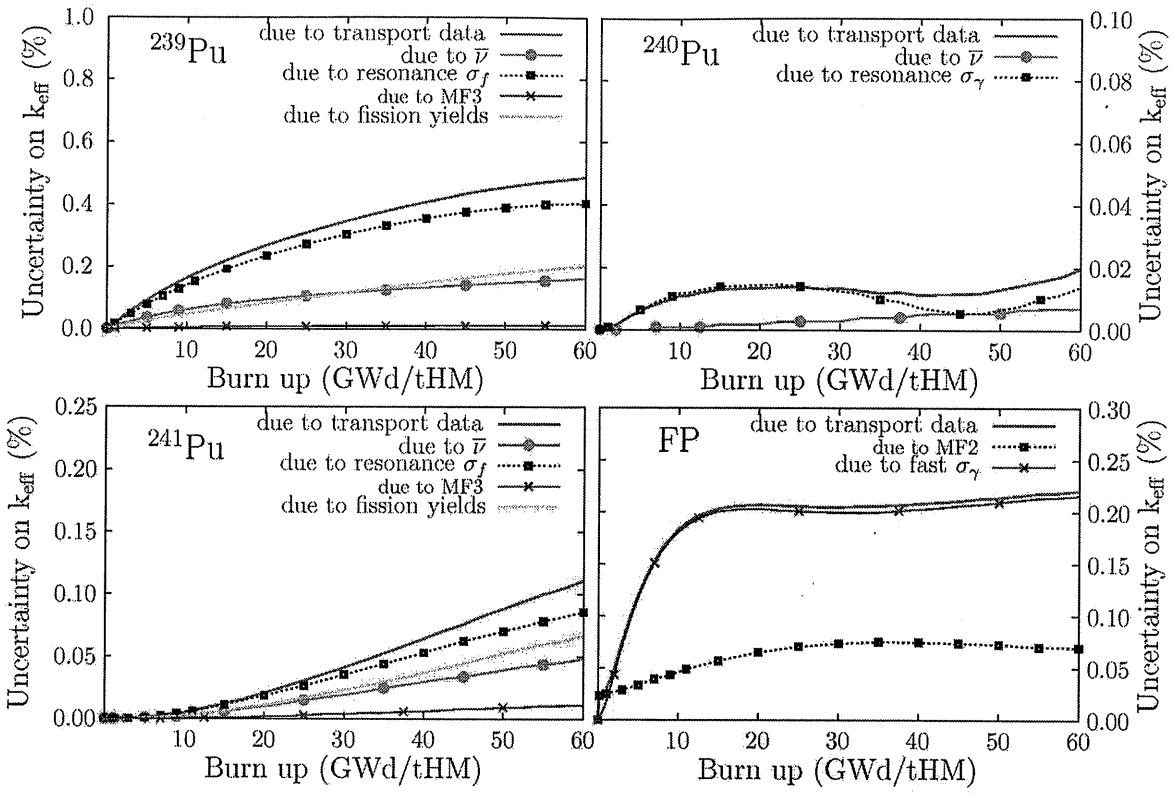

Fig. 6. Uncertainty in k_{eff} as a result of variations in nuclear data of various Pu isotopes and fission products (FP). Also shown are partial contributions (different MF numbers) to the total (labeled transport).

(52 pcm). When splitting the transport data contribution into its components, we notice that MF2 is the main contributor (70 pcm), followed closely by MF1 (39 pcm). As for ^{239}Pu, when we refer to variations in MF2 data, all resonance parameters are changed at the same time, but nevertheless the fission cross section is the main contributor to the total variation.

IV.B.3. Fission Products

Figure 6 also shows the effect on the final reactivity of the uncertainty in nuclear data for all fission products. During the first 15 GWd/tonne HM, the uncertainty increases very fast from an initial zero value (at BOL, no fission products are present in the fuel) to $\sim$200 pcm. Until the EOL, the uncertainty remains practically unchanged, although the amount of fission products increases steadily. The main contribution to the uncertainty can be attributed to the MF3, and more specifically to MT102, corresponding to radiative capture above the resonance range. The second most important contribution is from MF2 data. We should remark that this result is a combination of 128 isotopes, and they have different higher energy limits for the resonance range (typically, they can vary from $\sim$100 eV to $\sim$100 keV). This energy limit determines if the cross-section data are included in MF2 or in MF3. For this reason, we cannot state that the curve labeled as MF3 is associated exclusively with nuclear data for the fast energy range in the case of fission products. In the current study, the total uncertainty in k_{eff} of the grouped 128 fission products was not split into the different contributions, to identify the major sources of uncertainty. This will be the subject of a future study.

IV.B.4. Total Uncertainty

The contributions of the different isotopes considered to the uncertainty in k_{eff} are summarized in Table II (due to transport data) and Table III (due to fission yields) for a selection of burnup values. In the last column of Tables II and III, the different contributions are combined assuming that they are uncorrelated.

The total uncertainty in reactivity due to nuclear data can be quantified by combining the partial contributions of the different isotopes, according to the following procedure:

1. the contributions due to variations in transport data are combined assuming the contributions are uncorrelated
2. the contributions due to variations in fission yields are combined assuming the contributions are uncorrelated

TABLE II

Partial Uncertainties in k_{eff} Due to Variations in Transport Data of Different Isotopes

Burnup (GWd/tonne HM)	Uncertainty in k_{eff} Due to Transport Data of						Total Uncertainty (pcm)
	^{235}U (pcm)	^{238}U (pcm)	^{239}Pu (pcm)	^{240}Pu (pcm)	^{241}Pu (pcm)	FPs (pcm)	
0	536	458	0	0	0	0	705
10	447	441	163	12	5	183	674
20	396	406	268	21	21	207	661
40	331	322	407	37	64	208	654
50	299	321	454	43	88	214	674

TABLE III

Partial Uncertainties in k_{eff} Due to Variations in Fission Yields of Different Isotopes

Burnup (GWd/tonne HM)	Uncertainty Due to Fission Yields of				Total (pcm)
	^{235}U (pcm)	^{238}U (pcm)	^{239}Pu (pcm)	^{241}Pu (pcm)	
0	0	0	0	0	0
10	90	32	47	2	106
20	104	37	83	11	138
40	117	47	149	37	199
50	109	50	178	52	221

3. the two combined values for transport data and fission yields are combined, assuming they are either uncorrelated or correlated (fully or anticorrelated).

Figure 7 shows the combined uncertainty for transport data and fission yields, plotted as cumulative graphs. The lowest curve (labeled ^{235}U) represents the contribution for ^{235}U exclusively, the curve labeled ^{238}U represents the combined contribution of ^{238}U and ^{235}U, and so forth. The curve labeled FPs gives the combined contribution for all considered isotopes (^{235,238}U, ^{239,240,241}Pu, and all 127 fission products). We should point out that these graphs are an approximation, and the contribution of the different isotopes (as read from the *y*-axis) should not be seen as absolute values, except for the curve showing the total uncertainties. For the sake of graphical representation of the different contributions, the values of Tables II and III have been linearized.

The final uncertainty curve as a result of variations in transport data is reasonably flat and equal to 680 pcm. At BOL, only transport data from ^{235}U and ^{238}U deliver an important contribution. At EOL, the contributions of the different isotopes are more evenly distributed, and ^{239}Pu represent the largest effects, followed by ^{238}U, ^{235}U, and the combined fission products.

The curve in Fig. 8 represents the total combined uncertainty assuming the two contributions (of transport data and fission yields) are uncorrelated. The limits of the gray band denote the two extreme cases of either fully or anticorrelated. Also represented are points of previously reported calculations,[2,25–28] all based on application of the perturbation method for uncertainty propagation. The results reported here are, in general, in reasonable agreement with the previously reported values, although the TMC method includes the effect of variations in type of nuclear data not considered in the perturbation methods (because of the lack of covariance data).

Table IV includes the values of the two contributions (transport data and fission yields) at different burnup values. The total uncertainty is effectively constant with burnup, and amounts to 0.7%.

IV.C. Inventory

The uncertainty on the discharged masses for each isotope in the inventory was also studied, as result of variation in transport data and fission yields of the same isotopes. The final total uncertainty as a function of the

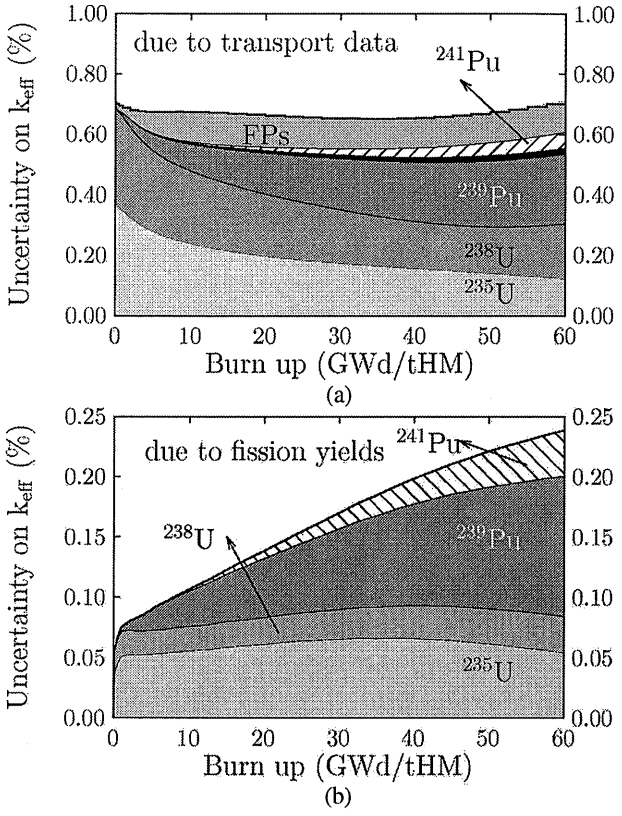

Fig. 7. Combined uncertainty on k_{eff} as a result of (a) transport data and (b) fission yields, plotted in a cumulative fashion.

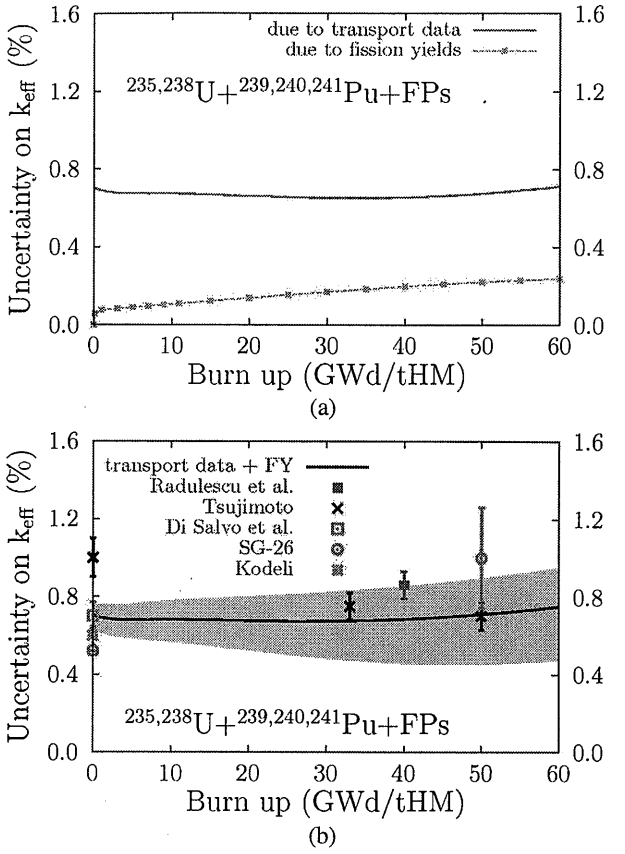

Fig. 8. (a) Total uncertainty as a result of variation in transport data and fission yields and (b) combined total uncertainty compared with literature data.

element is shown in Fig. 9, and Tables V and VI for discharge burnup of 50 GWd/tonne HM, where also the two contributions (transport data and fission yields) are displayed separately.[a] The lines represent the uncertainties averaged over the different isotopes of each particular element. The combination of the contributions was performed according to the same procedure as described in Sec. IV.B.4 for the uncertainties in reactivity.

IV.C.1. Fission Products Inventory

The uncertainties in inventory for fission products vary generally between 1% and 15%, except for some elements that are produced in small quantities in the fuel. The uncertainties for these elements (Ge, As, Se, In, Sn, Sb, Tb, and Dy, for example) are mostly in the range 10% to 35%. One exception is Zr, with high concentration because of the Zr-alloy cladding. The fuel cladding is homogenized together with the fuel and coolant before editing the inventory for the entire assembly. The uncertainty for this element is obviously rather small, since only a tiny amount is produced by fission.

[a]Tables V through VIII include detailed results for the uncertainty in inventory for the fission products and some important actinide isotopes, as a result of variations in transport data and fission yields. These two contributions are further summed up and included in the last columns of Tables V through VIII.

TABLE IV

Partial Uncertainties in k_{eff} as a Function of Fuel Burnup Due to Transport Data and Fission Yields, and Total Uncertainty

Burnup (GWd/tonne HM)	Uncertainty due to		Total Uncertainty (%)
	Transport (%)	Fission Yields (%)	
0	0.71	0.00	0.71
10	0.67	0.11	0.68
20	0.66	0.14	0.68
40	0.65	0.20	0.68
50	0.67	0.22	0.71

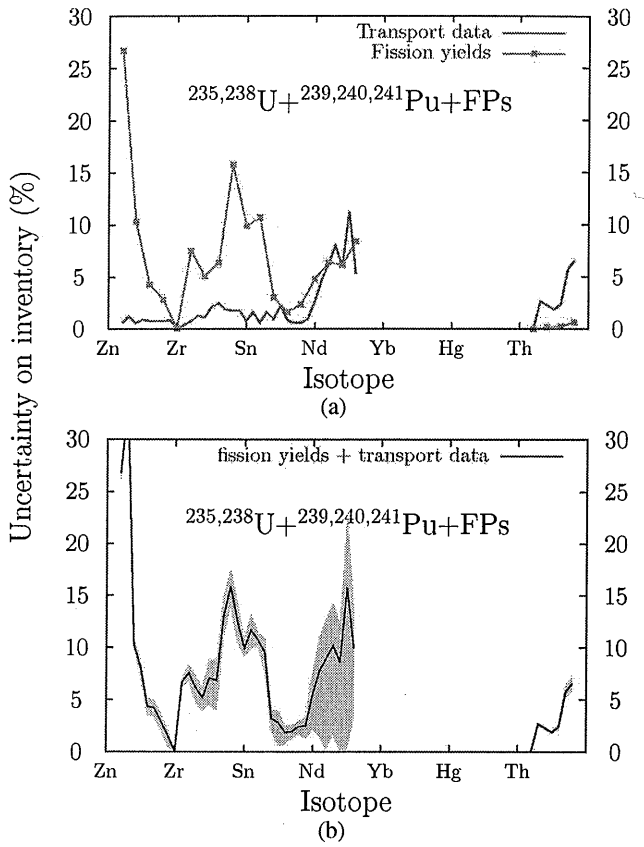

Fig. 9. Uncertainty in inventory at 50 GWd/tonne HM as a function of element due to (a) the variations in transport data and fission yields and (b) the combined effect.

For the fission products, the largest contribution is due to variations in fission yields, except for elements with $Z > 60$, for which the variations in transport data are as important as variations in fission yields. Figures 10a and 10c and Table VII give the separate contributions of the different isotopes, for the Z range of the fission products. In Fig. 10, the contributions are plotted in a cumulative fashion. For the element range Se-Y, the variations in fission yields of the main fissile isotopes ^{235}U and ^{239}Pu are the main contributors to the final uncertainty (in the range 1.5% to 10.5%). The fission yields of ^{235}U are mostly the main source of uncertainty for this element range. In the range Nb to Pr, the largest contributors are also the uncertainties in fission yields of ^{235}U and ^{239}Pu, with either one or the other being the most important depending on the particular element. In this element range, the total uncertainties lie in the range 2% to 16%. For elements in the range Nd to Dy, the main contributor is shared between the fission yields (of ^{235}U and ^{239}Pu) and the transport data for the fission products (the combined 128 fission products isotopes). The total uncertainty for this element range lies in the range 5.5% to 15%. At this stage of the study, we did not identify which fission products contribute the most to the total uncertainty.

IV.C.2. Actinides Inventory

For the actinide isotopes, the uncertainties are mostly below 5%, with the largest contribution due to variations in transport data (Fig. 9). Table VI gives the values of the uncertainties for the most important actinides with the partial contributions of transport data and fission yields. For the most relevant actinides, the uncertainties are in the range 1% to 3%. The separate contributions from the different isotopes are included in Table VIII and Figs. 10b and 10d. For most actinides, uncertainties in ^{235}U transport data are the largest source of uncertainty. For Pu, the uncertainties in ^{238}U transport data have the largest effect, whereas for Am and Cm, the data of ^{235,238}U and ^{239,241}Pu are equally important. For higher actinides like Bk and Cf, the importance of ^{235}U and ^{239}Pu dominates, followed by the contribution of ^{238}U.

To quantify the different sources of uncertainty in the inventory, the total uncertainty due to each separate isotope was split into the contributions of different reaction channels and other nuclear parameters included in the ENDF files. For this study, random files were applied where only a reduced number of reaction channels have changed, as performed for the study of uncertainties in reactivity. Figure 11 shows the contribution of the separate MF numbers (or particular reaction channels within each MF number) to the total contribution of each particular isotope (or groups of isotopes in the case of fission products).

Uncertainties in inventory of actinide isotopes due to variations in ^{235}U transport data are mainly attributed to uncertainties in data on MF2 (more specifically uncertainties on fission cross sections in the thermal and resonance range) and MF1 files (more specifically $\bar{\nu}$). Although comparable for some isotopes (in particular, for higher actinides), the contribution of variations in fission cross section is more important than the variations in $\bar{\nu}$.

In the case of variations in ^{238}U data, the isotopes ^{235}U, ^{239}Np, ^{239}Pu, ^{240}Pu, ^{241}Pu, and ^{241}Am are the most affected. The variations in MF2 data of ^{238}U (more specifically in radiative capture cross section in the thermal and resonance ranges) are the main source of uncertainties. These isotopes are produced by successive neutron capture and beta decay chains, except for ^{235}U, which is produced in small quantities by alpha decay of bred ^{239}Pu.

As ^{239}Pu transport data are varied, mostly the higher actinides are affected by them. The ^{239}Pu contribution is as important as the variations in ^{235}U (followed by ^{238}U). The results for the partial contributions of different MF numbers show that MF2 data are the main source of uncertainty, more specifically uncertainties in radiative capture cross sections in the thermal and resonance range. These higher actinides are produced by successive neutron capture followed by beta decay chains.

TABLE V

Uncertainties in Concentration of Fission Products as a Result of Combined Variations in Transport Data and Fission Yields for All Considered Isotopes and Combined Total Uncertainty*

Element	Yield (g/cm)	Uncertainty Due to		Total Uncertainty (%)
		Transport (%)	Fission Yields (%)	
Ge	3.52E−04[a]	0.57	26.71	26.72
As	1.17E−04	1.23	33.77	33.79
Se	3.58E−02	0.57	10.34	10.36
Br	1.42E−02	0.90	8.03	8.08
Kr	1.82E−01	0.79	4.31	4.38
Rb	1.67E−01	0.80	4.15	4.23
Sr	4.06E−01	0.77	2.82	2.92
Y	2.17E−01	0.85	1.31	1.56
Zr	3.35E+02	0.01	0.04	0.04
Nb	3.43E−02	0.39	6.66	6.67
Mo	2.74E+00	0.77	7.54	7.58
Tc	6.64E−01	1.28	6.04	6.17
Ru	2.76E+00	1.11	5.10	5.22
Rh	5.14E−01	2.12	6.76	7.09
Pd	2.09E+00	2.47	6.40	6.86
Ag	1.52E−01	1.89	12.93	13.07
Cd	1.76E−01	1.77	15.77	15.87
In	2.52E−03	1.80	12.39	12.52
Sn	9.80E−02	0.79	9.92	9.95
Sb	3.34E−02	1.61	11.55	11.66
Te	5.46E−01	0.61	10.72	10.74
I	2.59E−01	1.64	9.43	9.57
Xe	4.66E+00	0.95	3.05	3.19
Cs	2.48E+00	2.24	1.71	2.82
Ba	1.18E+00	0.87	1.64	1.85
La	1.02E+00	0.58	1.86	1.95
Ce	2.16E+00	0.59	2.35	2.43
Pr	8.73E−01	0.97	2.30	2.50
Nd	2.84E+00	2.66	4.78	5.47
Pm	1.54E−01	4.71	6.24	7.82
Sm	6.29E−01	6.27	6.42	8.97
Eu	1.88E−01	8.00	6.27	10.16
Gd	1.59E−01	6.00	6.14	8.59
Tb	6.18E−03	11.24	11.09	15.79
Dy	5.69E−03	5.28	8.44	9.96

*At 50 GWd/tonne HM.
[a]Read as 3.52×10^{-4}.

V. CONCLUSIONS

In this paper, the impact of the uncertainties in nuclear data of ^{235,238}U, ^{239,240,241}Pu, and the main fission products on reactivity and the discharged inventory of a typical PWR fuel assembly was quantified. This work builds on previous uncertainty studies by using the TMC method with the deterministic code DRAGON where the uncertainties in reactivity and inventory were analyzed as a result of variations in the ^{235,238}U isotopes. The basic DRAGON library is based on JEFF3.1 data, except for the isotopes being studied, the data of which are taken from TENDL-2012.

From the results of uncertainty in k_{eff}, we conclude the following:

1. Variations in transport data are the main source of uncertainty in reactivity both at BOL and EOL and amount to ~700 pcm. During burnup, the uncertainty remains virtually unchanged.

2. This value of uncertainty is in good agreement with values from the literature, calculated using the more traditional perturbation method.

3. At BOL, variations in the fission cross section in the thermal and resonance range of ^{235}U give the largest

TABLE VI

Uncertainties in Concentration of the Most Important Actinide Isotopes as a Result of Combined Variations in Transport Data and Fission Yields for All Considered Isotopes and Combined Total Uncertainty*

Element	Yield (g/cm)	Uncertainty Due to		Total Uncertainty (%)
		Transport (%)	Fission Yields (%)	
^{234}U	2.12E−01[a]	0.76	0.15	0.78
^{235}U	1.30E+01	1.96	0.53	2.03
^{236}U	7.93E+00	1.92	0.03	1.92
^{238}U	1.16E+03	0.04	0.00	0.04
^{237}Np	9.42E−01	2.91	0.16	2.92
^{239}Np	1.22E−01	0.97	0.08	0.98
^{238}Pu	4.00E−01	3.13	0.18	3.13
^{239}Pu	8.34E+00	2.73	0.21	2.73
^{240}Pu	3.67E+00	2.21	0.10	2.21
^{241}Pu	2.30E+00	1.73	0.16	1.74
^{242}Pu	9.90E−01	1.79	0.14	1.79
^{241}Am	7.09E−02	2.31	0.19	2.32
^{243}Am	2.33E−01	2.03	0.15	2.03
^{242}Cm	3.09E−02	1.19	0.12	1.19
^{244}Cm	9.66E−02	2.72	0.28	2.73

*At 50 GWd/tonne HM.
[a]Read as 2.12×10^{-1}.

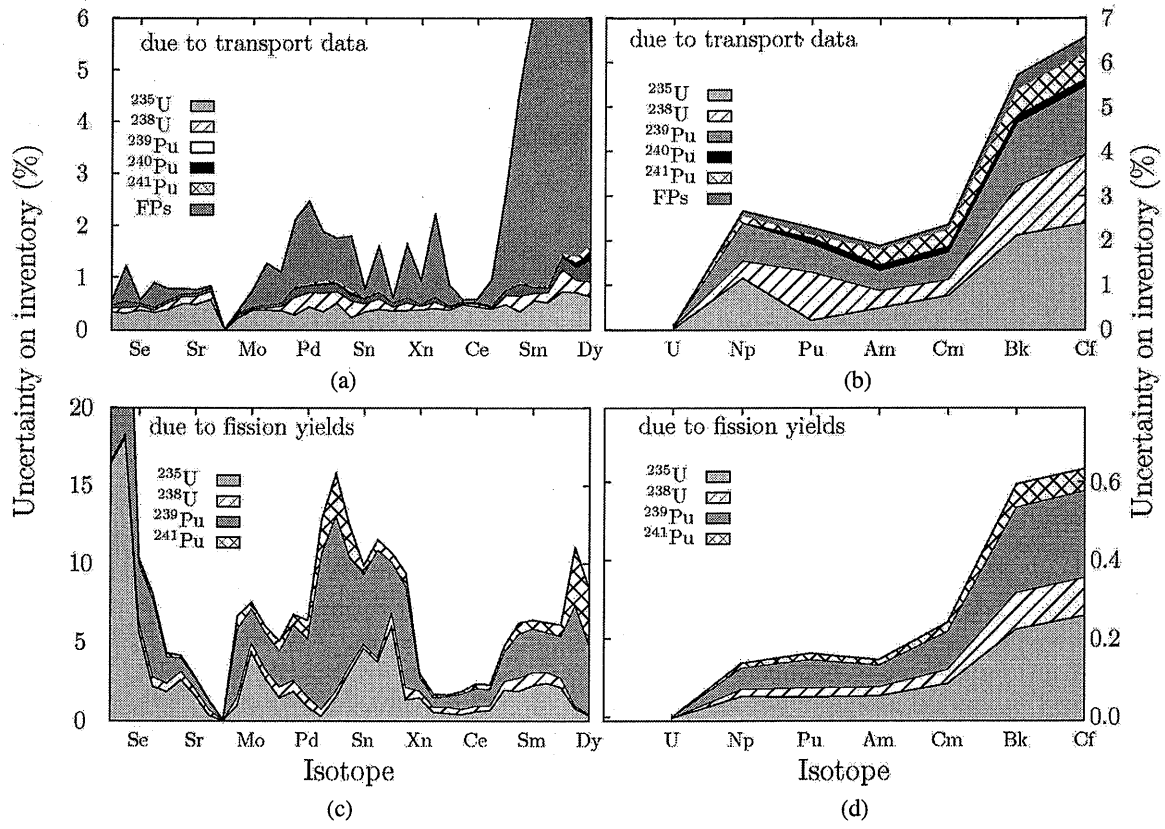

Fig. 10. Uncertainties in inventory (at 50 GWd/tonne HM) for (a, c) fission products and (b, d) actinides as a result of variations in (a, b) transport nuclear data and (c, d) fission yields. Contributions of the different isotopes are shown in all graphs.

TABLE VII

Uncertainties in Concentration of Fission Products as a Result of the Separate Variations in Transport Data and Fission Yields for Each of the Considered Isotopes*

Element	Yield (g/cm)	Uncertainty Due to										
		^{235}U		^{238}U		^{239}Pu		^{240}Pu		^{241}Pu		FPs
		Transport (%)	Fission Yields (%)	Transport (%)	Fission Yields (%)	Transport (%)	Fission Yields (%)	Transport (%)	Fission Yields (%)	Transport (%)	Fission Yields (%)	Transport (%)
Ge	3.52E−04[a]	0.54	23.20	0.12	0.25	0.09	13.20	0.01		0.03	1.06	0.11
As	1.17E−04	0.52	26.40	0.18	0.30	0.20	21.00	0.02		0.03	1.64	1.08
Se	3.58E−02	0.55	8.64	0.11	0.94	0.07	5.57	0.01		0.03	0.50	0.06
Br	1.42E−02	0.53	3.24	0.07	0.92	0.09	7.27	0.01		0.03	0.51	0.72
Kr	1.82E−01	0.67	3.10	0.23	0.92	0.09	2.82	0.01		0.02	0.43	0.35
Rb	1.67E−01	0.75	3.87	0.21	0.81	0.08	1.24	0.01		0.02	0.26	0.13
Sr	4.06E−01	0.73	2.50	0.22	0.69	0.08	1.09	0.01		0.02	0.13	0.07
Y	2.17E−01	0.81	0.59	0.22	0.69	0.09	0.94	0.01		0.02	0.14	0.03
Zr	3.35E+02	0.00	0.03	0.00	0.01	0.00	0.03	0.00		0.00	0.01	0.00
Nb	3.43E−02	0.37	1.40	0.07	0.77	0.07	6.35	0.01		0.05	1.20	0.02
Mo	2.74E+00	0.59	6.69	0.05	0.90	0.05	3.30	0.01		0.02	0.63	0.49
Tc	6.64E−01	0.55	4.49	0.07	0.97	0.08	3.86	0.01		0.02	0.70	1.15
Ru	2.76E+00	0.58	2.57	0.13	1.23	0.09	4.07	0.01		0.03	1.14	0.93
Rh	5.14E−01	0.44	3.07	0.52	1.21	0.26	5.80	0.03		0.03	1.10	1.99
Pd	2.09E+00	0.66	1.38	0.41	1.01	0.19	5.89	0.03		0.06	1.82	2.34
Ag	1.52E−01	0.60	0.35	0.63	0.57	0.27	12.60	0.04		0.08	2.81	1.65
Cd	1.76E−01	0.90	1.99	0.39	0.51	0.27	15.20	0.04		0.08	3.66	1.44
In	2.52E−03	0.38	4.91	0.53	0.59	0.17	10.90	0.06		0.10	3.22	1.67
Sn	9.80E−02	0.64	7.10	0.30	0.39	0.18	6.86	0.02		0.05	0.85	0.29
Sb	3.34E−02	0.66	5.51	0.34	0.35	0.19	10.10	0.04		0.06	0.98	1.41
Te	5.46E−01	0.57	9.32	0.13	1.37	0.12	5.03	0.01		0.03	0.96	0.11
I	2.59E−01	0.56	1.88	0.22	1.16	0.15	9.08	0.02		0.03	1.25	1.52
Xe	4.66E+00	0.62	2.50	0.12	0.73	0.06	1.52	0.01		0.03	0.43	0.71
Cs	2.48E+00	0.55	1.01	0.17	0.63	0.12	1.14	0.01		0.03	0.43	2.16
Ba	1.18E+00	0.60	0.82	0.06	0.74	0.05	1.20	0.00		0.03	0.17	0.62
La	1.02E+00	0.58	0.65	0.03	0.57	0.04	1.63	0.00		0.03	0.26	0.02
Ce	2.16E+00	0.58	1.01	0.08	0.64	0.04	1.95	0.00		0.03	0.55	0.05
Pr	8.73E−01	0.61	1.16	0.04	0.50	0.04	1.85	0.00		0.02	0.53	0.75
Nd	2.84E+00	0.66	3.36	0.25	0.97	0.12	3.18	0.01		0.03	0.68	2.56
Pm	1.54E−01	0.43	3.29	0.37	1.52	0.28	4.92	0.03		0.05	1.24	4.67
Sm	6.29E−01	0.64	3.86	0.17	1.45	0.13	4.83	0.02		0.04	0.93	6.23
Eu	1.88E−01	0.58	4.15	0.21	1.24	0.10	4.40	0.01		0.04	1.08	7.97
Gd	1.59E−01	0.96	3.69	0.56	1.04	0.30	4.62	0.03		0.08	1.28	5.89
Tb	6.18E−03	0.82	1.20	0.28	0.27	0.28	9.51	0.09		0.13	5.57	11.20
Dy	5.69E−03	0.90	0.49	0.40	0.10	0.59	6.45	0.16		0.21	5.42	5.15

*At 50 GWd/tonne HM.

[a]Read as 3.52×10^{-4}.

TABLE VIII

Uncertainties in Concentration of the Most Important Actinide Isotopes as a Result of Separate Variations in Transport Data and Fission Yields of the Considered Isotopes*

Isotope	Yield (g/cm)	Uncertainty Due to										
		^{235}U		^{238}U		^{239}Pu		^{240}Pu		^{241}Pu		FPs
		Transport (%)	Fission Yields (%)	Transport (%)	Fission Yields (%)	Transport (%)	Fission Yields (%)	Transport (%)	Fission Yields (%)	Transport (%)	Fission Yields (%)	Transport (%)
^{234}U	2.03E−01[a]	0.59	0.09	0.33	0.03	0.31	0.11	0.02		0.05	0.02	0.19
^{235}U	1.13E+01	1.19	0.52	1.42	0.05	0.62	0.11	0.04		0.08	0.02	0.16
^{236}U	8.32E+00	1.90	0.02	0.23	0.01	0.10	0.02	0.01		0.02	0.00	0.05
^{238}U	1.16E+03	0.02	0.00	0.04	0.00	0.01	0.00	0.00		0.00	0.00	0.00
^{237}Np	1.01E+00	2.28	0.12	0.68	0.03	1.64	0.10	0.03		0.32	0.02	0.18
^{239}Np	1.25E−01	0.36	0.04	0.77	0.02	0.42	0.07	0.04		0.11	0.02	0.18
^{238}Pu	4.38E−01	2.68	0.13	0.82	0.05	1.36	0.12	0.06		0.19	0.03	0.17
^{239}Pu	7.73E+00	0.23	0.13	2.45	0.05	1.12	0.15	0.04		0.03	0.04	0.35
^{240}Pu	3.72E+00	0.32	0.06	1.58	0.02	1.35	0.08	0.63		0.03	0.01	0.20
^{241}Pu	2.24E+00	0.21	0.09	1.49	0.04	0.76	0.12	0.26		0.22	0.03	0.17
^{242}Pu	1.10E+00	0.97	0.10	0.32	0.04	1.00	0.09	0.27		1.03	0.02	0.09
^{241}Am	6.62E−02	0.24	0.12	2.21	0.05	0.50	0.13	0.29		0.19	0.03	0.23
^{243}Am	2.61E−01	1.30	0.11	0.44	0.04	1.11	0.09	0.27		0.95	0.02	0.15
^{242}Cm	3.21E−02	0.57	0.08	0.62	0.03	0.76	0.08	0.28		0.19	0.02	0.09
^{244}Cm	1.14E−01	1.89	0.19	0.79	0.07	1.43	0.19	0.29		1.00	0.05	0.25

*At 50 GWd/tonne HM.
[a]Read as 2.03×10^{-1}.

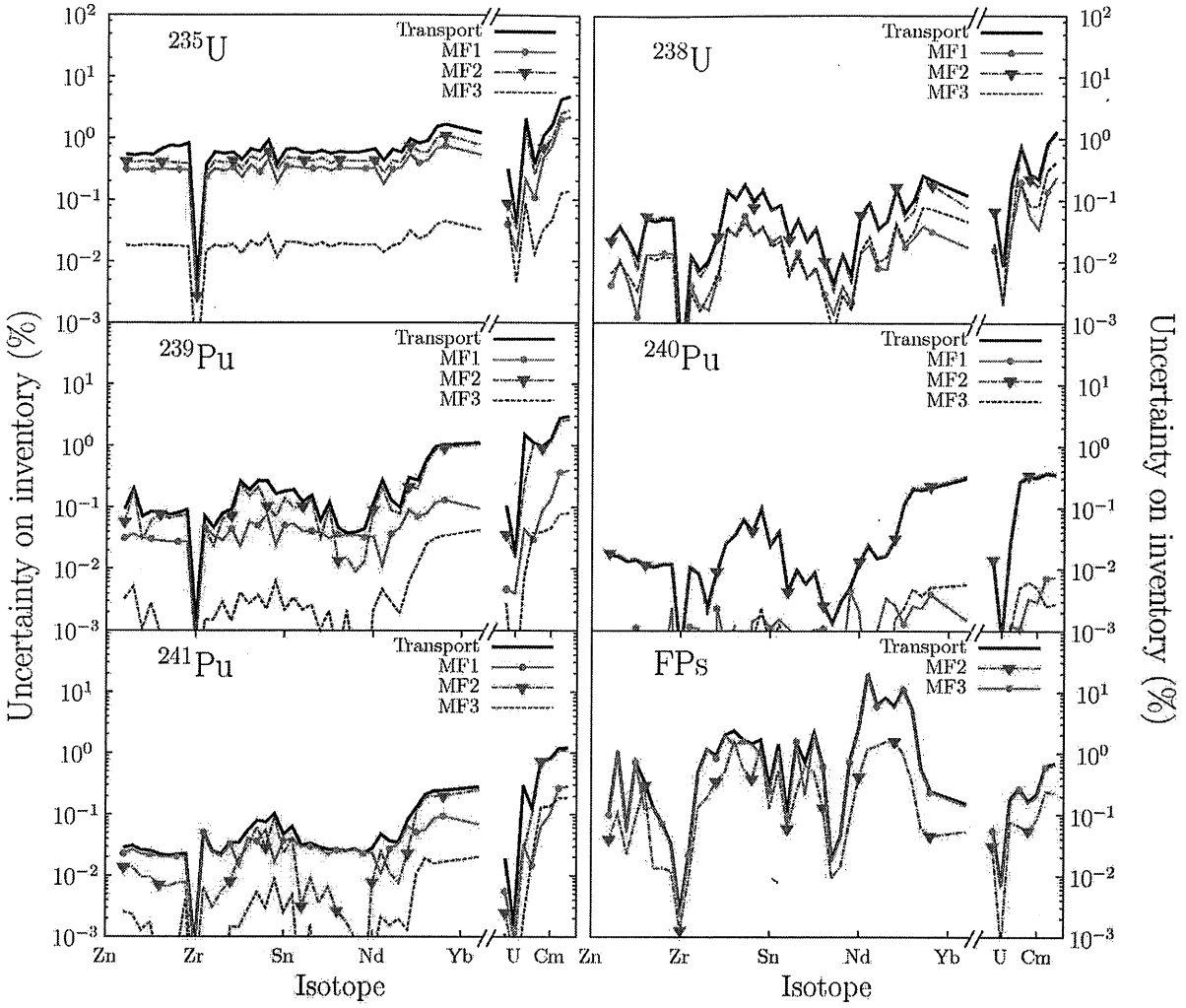

Fig. 11. Uncertainty in inventory (at 50 GWd/tonne HM) as a result of variations in nuclear transport data of different isotopes. Also shown is the partial contribution of different nuclear data types (MF numbers).

effect, followed by uncertainties in resonance radiative capture and $\bar{\nu}$ in ^{238}U.

4. At EOL, the uncertainties in ^{235}U, ^{239}Pu, and ^{238}U are equally important. The main contributors are fission cross section in the thermal and resonance range (from ^{235}U and ^{239}Pu), and radiative capture (in the resonance and thermal range) and $\bar{\nu}$ from ^{238}U.

5. The effect on k_{eff} of uncertainties in fission products data is of secondary importance. However, at EOL, its contribution is larger than 70% of the effect of the uncertainties due to the ^{235}U data.

From the results of uncertainty in discharged inventory at 50 GWd/tonne HM we conclude that:

1. For most fission products, the total uncertainty in their concentration is in the range 1% to 15%. The most important contribution is from uncertainties in fission yields from the main fissile isotopes: ^{235}U and ^{239}Pu.

2. Important quantities not considered in this study, but directly related to the discharged inventory, are the radiotoxicity and heat source. Some of the fission products in the elemental range $Z \leq 60$ represent important sources of heat and toxicity either at short (Cs and Sr, for example) or long term (Tc and I, for example). As discussed above, the main sources of uncertainties in the inventory for these fission products are attributed to uncertainties in the fission yields of ^{235}U and ^{239}Pu. Therefore, it is important that these uncertainties are properly addressed by the nuclear data community.

3. For the actinides, the uncertainties are mostly below 5%, with the largest source of uncertainty being the transport data of ^{235}U, ^{238}U, and ^{239}Pu (and to a lesser extent ^{241}Pu). In the case of ^{235}U and ^{239}Pu data, uncertainties in data on MF2 (more specifically, the fission cross section in the thermal and resonance range) and MF1 (mainly $\bar{\nu}$) give the largest contributions. For

^{238}U, mainly uncertainties in MF2 data (more specifically, radiative capture cross section in the thermal and resonance range) give the major contributions.

4. For both the fission products and actinides isotopes, the effects of uncertainties due to the fission products nuclear data are of secondary importance, except for the fission products with $Z \geq 60$. In this elemental range, variations in MF3 data are the main source of uncertainties (together with variations in ^{235}U and ^{239}Pu fission yields).

We noticed from the analysis that the major contributors to the uncertainty in k_{eff} are not always the ones that contribute the most to the uncertainty in the inventory.

So far, only the most important actinides have been considered in this study, whereas (dependent on their uncertainty) some minor actinides can be also of importance, certainly at high burnup values. Other light elements (structural and in the coolant, like H, O, B, and Zr) have also not been considered. A follow-up study should include some of these important isotopes. After that, the nuclear data themselves may be optimized.

APPENDIX

LIST OF FISSION PRODUCTS

TABLE A.I

List of Fission Products with Randomized Nuclear Data

No.	Nuclide	No.	Nuclide	No.	Nuclide	No.	Nuclide
1	32-Ge-72	35	44-Ru-104	69	53-I-129	103	62-Sm-150
2	32-Ge-73	36	44-Ru-106	70	53-I-135	104	62-Sm-151
3	32-Ge-74	37	45-Rh-103	71	54-Xe-128	105	62-Sm-152
4	32-Ge-76	38	45-Rh-105	72	54-Xe-130	106	62-Sm-154
5	33-As-75	39	46-Pd-104	73	54-Xe-131	107	63-Eu-151
6	34-Se-76	40	46-Pd-105	74	54-Xe-132	108	63-Eu-152
7	34-Se-77	41	46-Pd-106	75	54-Xe-134	109	63-Eu-153
8	34-Se-78	42	46-Pd-107	76	54-Xe-135	110	63-Eu-154
9	34-Se-80	43	46-Pd-108	77	54-Xe-136	111	63-Eu-155
10	34-Se-82	44	46-Pd-110	78	55-Cs-133	112	64-Gd-152
11	35-Br-79	45	47-Ag-109	79	55-Cs-134	113	64-Gd-154
12	35-Br-81	46	48-Cd-111	80	55-Cs-135	114	64-Gd-155
13	36-Kr-80	47	48-Cd-112	81	55-Cs-137	115	64-Gd-156
14	36-Kr-82	48	48-Cd-113	82	56-Ba-134	116	64-Gd-157
15	36-Kr-83	49	48-Cd-114	83	56-Ba-135	117	64-Gd-158
16	36-Kr-84	50	48-Cd-116	84	56-Ba-136	118	64-Gd-160
17	36-Kr-86	51	49-In-113	85	56-Ba-137	119	65-Tb-159
18	37-Rb-85	52	49-In-115	86	56-Ba-138	120	65-Tb-160
19	37-Rb-87	53	50-Sn-115	87	58-Ce-140	121	66-Dy-160
20	38-Sr-86	54	50-Sn-117	88	58-Ce-142	122	66-Dy-161
21	38-Sr-87	55	50-Sn-118	89	59-Pr-141	123	66-Dy-162
22	38-Sr-88	56	50-Sn-119	90	60-Nd-142	124	66-Dy-163
23	39-Y-89	57	50-Sn-126	91	60-Nd-143	125	66-Dy-164
24	40-Zr-93	58	51-Sb-121	92	60-Nd-144	126	67-Ho-165
25	41-Nb-94	59	51-Sb-123	93	60-Nd-145	127	68-Er-166
26	42-Mo-95	60	51-Sb-125	94	60-Nd-146	128	68-Er-167
27	42-Mo-96	61	52-Te-122	95	60-Nd-148		
28	42-Mo-97	62	52-Te-123	96	60-Nd-150		
29	43-Tc-99	63	52-Te-124	97	61-Pm-147		
30	44-Ru-99	64	52-Te-125	98	61-Pm-148		
31	44-Ru-100	65	52-Te-126	99	61-Pm-149		
32	44-Ru-101	66	52-Te-128	100	62-Sm-147		
33	44-Ru-102	67	52-Te-130	101	62-Sm-148		
34	44-Ru-103	68	53-I-127	102	62-Sm-149		

REFERENCES

1. L. L. BRIGGS, "Status of Uncertainty Quantification Approaches for Advanced Reactor Analyses," ANL-GenIV-110, Argonne National Laboratory (2008).

2. M. SALVATORES et al., "Uncertainty and Target Accuracy Assessment for Innovative Systems Using Recent Covariance Data Evaluations," Report by the Working Party on International Evaluation Cooperation of the NEA Nuclear Science Committee, NEA0WPEC-26, Vol. 26, Nuclear Energy Agency, Organisation for Economic Co-operation and Development (2008).

3. G. ALIBERTI et al., "Nuclear Data Sensitivity, Uncertainty and Target Accuracy Assessment for Future Nuclear Systems," *Ann. Nucl. Energy*, **33**, 700 (2006); http://dx.doi.org/10.1016/j.anucene.2006.02.003.

4. A. J. KONING and D. ROCHMAN, "Towards Sustainable Nuclear Energy: Putting Nuclear Physics to Work," *Ann. Nucl. Energy*, **35**, 2024 (2008); http://dx.doi.org/10.1016/j.anucene.2008.06.004.

5. J. LEPPANEN, "PSG2/Serpent—A Continuous-Energy Monte Carlo Reactor Physics Burnup Calculation Code," VTT Technical Research Center, Finland (2010); http://montecarlo.vtt.fi (current as of Nov. 2, 2012).

6. "MCNP—A General Monte Carlo N-Particle Transport Code," J. F. BRIESMEISTER, Ed., Version 4C, LA-13709-M, Los Alamos National Laboratory (2000).

7. D. ROCHMAN, A. J. KONING, and D. F. DA CRUZ, "Propagation of ^{235,236,238}U and ^{239}Pu Nuclear Data Uncertainties for a Typical PWR Fuel Element," *Nucl. Technol.*, **179**, 323 (2012).

8. D. F. DA CRUZ, D. ROCHMAN, and A. J. KONING, "Uncertainty Analysis on Reactivity and Discharged Inventory for a Pressurized Water Reactor Fuel Assembly Due to ^{235,238}U Nuclear Data Uncertainties," *Proc. Int. Congress on Advances in Nuclear Power Plants (ICAPP 2012)*, Chicago, Illinois, June 24–28, 2012.

9. J. J. DUDERSTADT and L. J. HAMILTON, *Nuclear Reactor Analysis*, Appendix H, Wiley & Sons, New York (1976).

10. G. MARLEAU, R. ROY, and A. HEBERT, "DRAGON: A Collision Probability Transport Code for Cell and Supercell Calculations," IGE–157, Ecole Polytechnique de Montreal (1993).

11. A. HEBERT, G. MARLEAU, and R. ROY, "Application of the Lattice Code DRAGON to CANDU Analysis," *Trans. Am. Nucl. Soc.*, **72**, 335 (1995).

12. "WIMS-D Library Update: Final Report of a Coordinated Research Project," STI/PUB/1264, International Atomic Energy Agency, Vienna, Austria (May 2007).

13. A. J. KONING, S. HILAIRE, and M. C. DUIVESTIJN, "TALYS-1.0," *Proc. Int. Conf. Nuclear Data for Science and Technology*, Nice, France, April 23–27, 2007.

14. D. ROCHMAN and A. J. KONING, "Pb and Bi Neutron Data Libraries with Full Covariance Evaluation and Improved Integral Tests," *Nucl. Instrum. Methods Phys. Res. A*, **589**, 85 (2008); http://dx.doi.org/10.1016/j.nima.2008.02.003.

15. A. J. KONING and D. ROCHMAN, "Modern Nuclear Data Evaluation with the TALYS Code System," *Nucl. Data Sheets*, **113**, 2841 (2012); http://dx.doi.org/10.1016/j.nds.2012.11.002

16. D. ROCHMAN and C. M. SCIOLLA, "Total Monte Carlo—Uncertainty Propagation Applied to the Phase I-1 Burnup Calculation," NRG Report 113690, Nuclear Research and Consultancy Group (2012).

17. A. C. WAHL, "Systematics of Fission-Products Yields," LA-13928, Los Alamos National Laboratory (May 2002).

18. R. MacFARLANE and D. M. MUIR, "The NJOY Nuclear Data Processing System, Version 91," LA-17740, Los Alamos National Laboratory (1994).

19. C. J. DEAN and R. J. PERRY, "Weighting Spectra for the XMAS Group Scheme," Winfrith Technology Center, August 8, 1990.

20. A. HÉBERT and A. SANTAMARINA, "Refinement of the Santamarina-Hfaiedh Energy Mesh Between 22.5 eV and 11.4 keV," *Proc. Int. Conf. Physics of Reactors*, Interlaken, Switzerland, September 14–19, 2008.

21. A. J. KONING and D. ROCHMAN, "TENDL-2009: Consistent TALYS-Based Evaluated Nuclear Data Library Including Covariance Data," NEA/WPEC JEF-DOC-1310, NEA Nuclear Data Bank, Paris, France (2009); http://www.talys.eu/tendl-2011 (current as of Nov. 2, 2012).

22. H. HENDRIKSON et al., "The Art of Collecting Experimental Data Internationally: EXFOR, CINDA and the NRDC Network," *Proc. Int. Conf. Nuclear Data for Science and Technology*, Nice, France, April 23–27, 2007, p. 197.

23. S. F. MUGHABGHAB, *Atlas of Neutron Resonances*, 5th ed., Elsevier, Amsterdam, The Netherlands (2006).

24. D. ROCHMAN and A. J. KONING, "Evaluation and Adjustment of the Neutron-Induced Reactions of ^{63,65}Cu," *Nucl. Sci. Eng.*, **170**, 265 (2012).

25. G. RADULESCU, D. E. MUELLER, and J. C. WAGNER, "Sensitivity and Uncertainty Analysis of Commercial Reactor Criticals for Burnup Credit," *Nucl. Technol.*, **167**, 268 (2009).

26. J. DI SALVO, et al., "Nuclear Data Uncertainty Propagation on the Jules Horowitz Reactor Neutronic Parameters," *Proc. Reactor Physics, Safety and High-Performance Computing Conf. (PHYSOR 2002)*, Seoul, Korea, October 7–10, 2002.

27. K. TSUJIMOTO, "Nuclear Data Needs for Accelerator Driven Transmutation System," *Proc. Specialists' Mtg. Reactor Group Constants*, Tokai, Japan, February 22–23, 2001, JAERI-Conf. 2001-009, p. 41.

28. I. KODELI and L. SNOJ, "Evaluation and Uncertainty Analysis of the KRITZ-2 Critical Benchmark Experiments," *Nucl. Sci. Eng.*, **171**, 231 (2012).